Nuclear Physics A282 (1977) 243—268; © *North-Holland Publishing Co., Amsterdam*

ROTATIONAL STRUCTURES IN DOUBLY ODD ^{198}Tl

A. J. KREINER† and M. FENZL

Physik-Department der Technischen Universität München, E17, 8046 Garching, Germany††

S. LUNARDI

Institut für Kernphysik, Kernforschungsanlage Jülich, D-517 Jülich, Germany

and

M. A. J. MARISCOTTI

Departamento de Fisica Nuclear, Comision Nacional de Energia Atomica, Buenos Aires, Argentina

Received 3 December 1976

Abstract: States of ^{198}Tl, excited through the ^{197}Au(α,3n) reaction at $E_\alpha = 30$ to 55 MeV, were studied using in-beam γ-spectroscopic techniques. Excitation functions, γ-ray angular distributions, γ-γ coincidences, half-lives in the nsec and μsec regions and conversion electron spectra were measured. As expected, due to the different type of experiment, a completely new scheme was found as compared to the known data. Two "rotational-like" structures were found based on isomeric states at 934.3 keV ($I^\pi = 8^-$, $T_{\frac{1}{2}} = 12.3 \pm 0.3$ nsec) and 687.1 keV ($I^\pi = (5)^+$, $T_{\frac{1}{2}} = 150 \pm 40$ nsec). The intrinsic structure of the band based on the 8^- isomer is interpreted as being the coupling of a $\tilde{h}_{\frac{9}{2}}$ proton strongly coupled to the nuclear symmetry axis and a rotation-aligned $i_{\frac{13}{2}}$ quasi-neutron. A diagonalization of the particle-rotation coupling Hamiltonian within the $\tilde{\pi}h_{\frac{9}{2}} \otimes \nu i_{\frac{13}{2}}$ configuration space lends support to this description.

E NUCLEAR REACTION ^{197}Au(α, 3nγ), $E = 30$–55 MeV; measured E_γ, I_γ, $\sigma(E_\alpha, E_\gamma, \theta_\gamma, t)$, γ-γ coin, I_{ce}. ^{195}Tl deduced levels. J, π, $T_{\frac{1}{2}}$, ICC, γ-mixing. Ge(Li) detectors, orange β-spectrometer.

1. Introduction

Doubly odd thallium isotopes have been investigated in the past mainly through the electron capture decay of the ground states of the corresponding lead isotopes [1,2]). In this process only the low energy, low-spin part of the spectra are reached. Also some studies concerning high-spin long-lived isomers have been carried out through (p, n) [ref. [3])] and (HI, xn) [ref. [4])] reactions. From this work, the γ-decay of these 7^+ states to the ground state is known. Until now no in-beam measurements of the prompt γ-rays following the production of these nucleides have been made. On the contrary, the situation is very different in the odd-mass thallium nuclei. Many of them have been studied with heavy-ion reactions [5, 6]). There exists now very well established evidence for the existence of rotational bands based on the $\frac{9}{2}^-$[505] proton

† On leave of absence from Departamento de Fisica Nuclear, Comision Nacional de Energia Atomica, Buenos Aires, Argentina.

†† This work was partly supported by the DAAD (Deutscher Akademischer Austauschdienst).

Nilsson state with oblate deformation. These states display the right features as to allow an interpretation in terms of a so-called strongly coupled band. This is the typical situation for a particle well above the Fermi surface coupled to an oblate core [7]).

A very interesting phenomenon takes place here, which can be understood as a shape transition. Thallium is spherical in the ground state; it is just one single hole in a lead core. When the odd proton jumps to the next higher-lying major shell we are left with a Hg core and the extra polarizing effects of the particle in the high-single-j equatorial orbital ($j_p^\pi = \frac{9}{2}^-$, $\Omega_p = \frac{9}{2}$). In this situation it is energetically more favourable for the system to adopt a certain permanent oblate deformation, although it is not clear up to now to what extent the wave function is spread out in the β-γ plane [8]). We believe now that it is very likely that such a behaviour is also realized in even-mass thallium nuclei.

2. Experimental procedures and results

The experimental information presented in this paper is the result of work done in three different laboratories. The first set of experiments has been performed with the α-particle beam from the Buenos Aires synchrocyclotron at the AEC of Argentina. This work comprises the measurement of γ-ray excitation functions, activity spectra, a preliminary run of γ-γ coincidences and the search for isomerism in the μsec region, making use of the natural time structure of the beam. The second one was done with a similar beam from the Jülich isochronous cyclotron. The γ-ray angular distributions, γ-γ coincidences and time distributions in the nsec region were obtained. Conversion electron spectra were measured at the Bonn University variable energy cyclotron making use of the orange β-spectrometer facility.

2.1. EXCITATION FUNCTION MEASUREMENTS

The usual way to do a preliminary isotopic assignment of the different γ-rays following a (HI, xn) reaction is to measure their yield as a function of the bombarding energy. In heavy mass nuclei and at not too high excitation energies of the compound system, reactions which involve only neutrons in the exit channel are by far the predominant ones. In addition the cross sections for reactions which differ in one evaporated neutron are very well separated [9]) and have characteristic shapes so that the identification on this basis, especially in the case of a monoisotopic target, is almost certain. With the aid of a beam degrading device, consisting essentially of aluminium absorber foils of different thicknesses, a 6 mg/cm^2 gold target was irradiated with an α-particle beam of energies ranging from 30 to 55 MeV in 5 MeV steps. A 30 cm^3 Ge(Li) detector of about 3 keV resolution for the 1.33 MeV ^{60}Co line has been used. Spectra were accumulated both during and between the beam bursts, using a gate signal derived from the frequency-modulation system of the synchrocyclotron, in order to get cleaner, activity-free spectra for the in-beam part and also to make a first search for lifetimes greater than a few μsec. The (α, 3n) reaction was found to peak at an

energy around 35 MeV. Fig. 1 shows a spectrum taken at his energy with the detector at 90° to the beam direction, it includes both in- and out-of-beam contributions.

2.2. ANGULAR DISTRIBUTION MEASUREMENTS

The spectra for the angular distribution measurements were taken at six angles between 90° and 165° in 15° steps. The details of the set-up are described in ref. [10]). A 40 cm^3 Ge(Li) (FWHM = 0.95 keV at 122 keV) was used as the moving detector, shielded with an Ta-Cd-Cu absorber sandwich of optimized thicknesses to reduce the strong X-ray intensities. A second fixed 12 cm^3 Ge(Li) detector placed at 45° was used

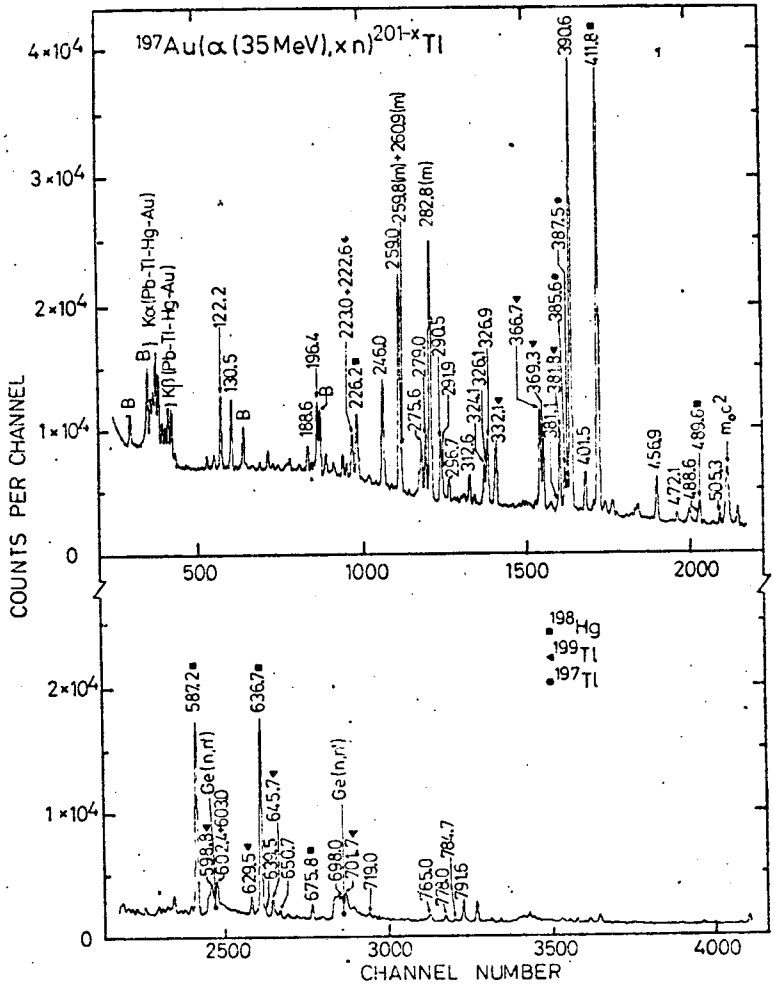

Fig. 1. Singles γ-ray spectrum from the ^{197}Au(α, xn)$^{201-x}$Tl reaction at $E_\alpha \approx 35$ MeV. Lines labelled only with their energies represent transitions in ^{198}Tl. The symbol (m) denotes lines coming from the decay of ^{198m}Tl. The letter B indicates background peaks.

TABLE 1

The ^{198}Tl γ-ray energies, angle integrated γ-intensities and angular distribution coefficients in the ^{197}Au(α, 3n) reaction at $E_\alpha \approx 35$ MeV.

E_γ (keV) [a]	I_γ	A_2/A_0	A_4/A_0
111.2	2.5±0.3	−0.75±0.07	0.3 ±0.1
115.8	2.0±0.3		
116.8	2.9±0.2	−0.50±0.07	0.0 ±0.1
122.2	18.4±0.9	−0.41±0.02	0.03±0.03
130.5	18.7±0.9	−0.20±0.02	−0.07±0.03
143.5	1.2±0.5		
188.6	4.7±0.2	−0.45±0.05	−0.08±0.06
196.4	14.8±1.0	−0.64±0.05	−0.08±0.05
223.0	7.3±0.7	−0.30±0.05	−0.04±0.04
246.0	21.0±1.0	−0.49±0.02	−0.06±0.03
259.0	44.0±2.0	−0.48±0.02	−0.10±0.03
259.9 [b]	8.0±1.0		
275.6	11.2±0.5	−0.58±0.02	−0.01±0.02
279.0	13.9±0.7	−0.45±0.02	0.01±0.02
282.8 [b]	67.0±3.0		
290.5	13.1±0.6	−0.45±0.02	0.04±0.03
291.9	6.6±0.3 [c]	0.24±0.03	−0.19±0.04
296.7	4.6±0.3	−0.56±0.04	−0.01±0.04
303.7	1.5±0.5		
312.6	6.3±0.3	−0.71±0.04	0.07±0.05
316.1	1.9±0.2	−0.58±0.09	0.09±0.12
324.1	9.3±0.5	−0.57±0.05	0.06±0.05
326.1	13.0±1.0	0.36±0.20	−0.2 ±0.2
326.9	12.0±1.0	−0.6 ±0.2	0.3 ±0.2
381.1	3.8±0.6	0.28±0.16	0.30±0.26
390.6	156.0±8.0	−0.28±0.02	−0.06±0.03
401.5	12.3±0.6	−0.56±0.02	−0.03±0.03
456.8	16.5±1.0	−0.73±0.02	0.05±0.03
472.1	5.7±0.3	0.28±0.06	−0.15±0.08
488.6	3.3±0.3	−0.2 ±0.1	0.3 ±0.2
505.3	5.5±0.3	0.11±0.08	−0.3 ±0.2
602.4 [c]	4.3±0.6	0.18±0.20	
603.0 [c]	11.0±1.0	0.4 ±0.2	
639.5	5.9±0.3	0.36±0.05	−0.02±0.06
647.7 [c]	4.0±0.4	0.15±0.08	
650.7	5.1±0.3	0.32±0.05	−0.10±0.07
698.2 [c]	3.0±0.3	0.4 ±0.1	
719.0	1.7±0.2	0.6 ±0.1	−0.2 ±0.2
765.0	4.5±0.4	−0.13±0.06	0.04±0.08
778.1	6.5±0.5	0.37±0.05	0.15±0.06
784.7	2.0±0.4		
791.6	10.9±0.7	−0.77±0.03	0.03±0.04

[a] $0.1 \leqq |\Delta E_\gamma| \leqq 0.2$ keV.

[b] These transitions are only fed through the 7^+ isomer ($T_{\frac{1}{2}} = 1.87$ h), its intensities depend on details of the irradiation.

[c] The fit was performed with the constraint $A_4 = 0$.

for normalization purposes. Several in-beam peaks in the 12 cm^3 spectra were evaluated for each angle and the sums were taken as the normalization constants. In addition corrections for dead-time losses were performed. This method has the advantage over the classical pulser procedure that contributions from induced radioactivity which are not proportional to the beam current are excluded. The whole angular range was covered three times and the corresponding spectra were summed up for the subsequent analysis. Table 1 shows the results obtained from this analysis for those γ-rays which belong to ^{198}Tl. The I_γ represent the angle integrated intensities, A_2/A_0 and A_4/A_0 are the experimental angular distribution coefficients, i.e. with the attenuation factors included. Fig. 2 shows some angular distributions of dipole character for the cascade ending on the state depopulated by the 390.6 keV transition.

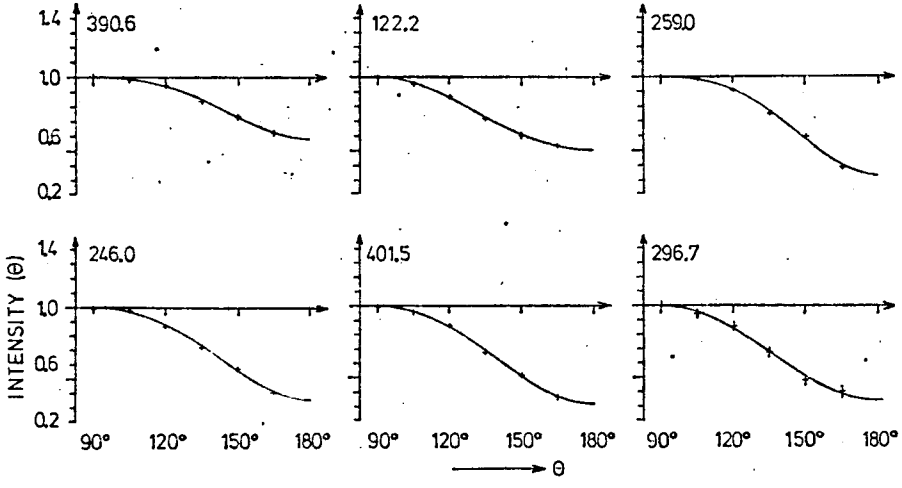

Fig. 2. Experimental angular distributions of dipole-type transitions in the negative parity band.

One can see how the anisotropy becomes more pronounced as one proceeds towards higher excitation energies. In order to do spin assignments and to extract the quadrupole mixing ratios a $\chi^2(\delta)$ fit to the data was performed.

2.3. THE γ-γ COINCIDENCE EXPERIMENT

The coincidence data are the most powerful tool for constructing a level scheme. To get arguments of comparable quality from energy sums and intensity balance the precision of those measurements has to be improved significantly over the present status.

The definitive runs at Jülich were carried out with two Ge(Li) detectors of 71 cm^3 (3 keV FWHM at 1.33 MeV) and 40 cm^3 (1 keV FWHM at 122 keV) positioned at 125° and 140° with respect to the beam direction. The coincidence rate was about 1 kHz. The employed technique is described in ref. [11]). For each event converting

within the $t_{\gamma\gamma}$ time to amplitude converter (TAC) range the four coordinates (E_{γ_1}, E_{γ_2}, $t_{\gamma_1\gamma_2}$, $t_{\gamma_1 RF}$) (i.e. γ-ray energies in the 71 and 40 cm^3 detectors, time between them and time between the radiofrequency pulse and the arrival of the γ-quantum in the 71 cm^3 detector) were digitalized in a (2K × 2K × 1K × 1K) matrix in four different ADC units, recorded on magnetic tape and sorted afterwards. Fig. 3 shows some of the coincidence spectra with gates set on members of the strongest cascade ending on the 12 nsec isomer, these are prompt coincidences. The first spectrum from below

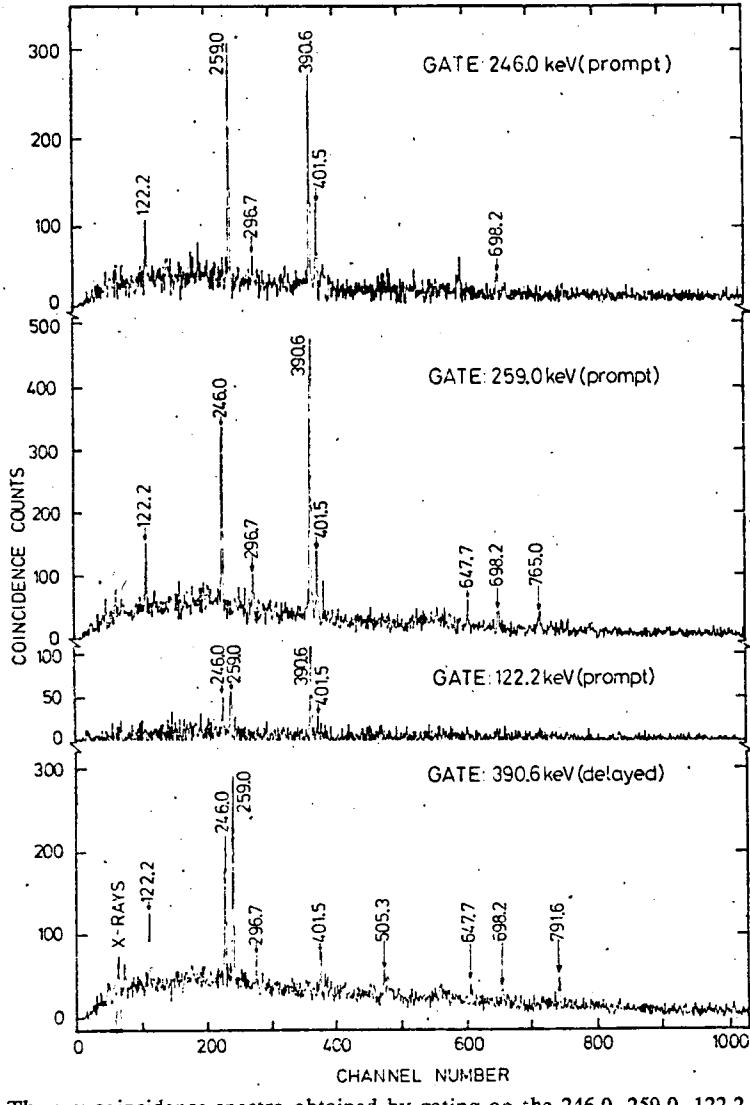

Fig. 3. The γ-γ coincidence spectra obtained by gating on the 246.0, 259.0, 122.2 and 390.6 keV lines. The first spectrum from below corresponds to a time window on the delayed side of the $t_{\gamma\gamma}$ TAC curve, the other ones represent prompt coincidences.

corresponds to a gate set on the isomeric transition and with the time window displaced to the delayed side of the $t_{\gamma\gamma}$ curve (this is the reason for the somewhat lower intensity). Essentially two independent families of γ-rays could be found. Tables 2 and 3 show the results from a quantitative evaluation of all coincidence spectra. A coincidence efficiency calibration has been performed with a ^{152}Eu source. Table 2 gives the results for the set of γ-rays which precede the 390.6 keV transition and table 3 for those which are in prompt and delayed coincidence with the 130.5 keV γ-ray.

As a consequence of the great complexity of the spectra, not only because of the large number of transitions but also and especially due to the presence of many interrelated double and triple lines, the sorting procedure became a very extensive task. In some cases it was necessary to scan the lines channel by channel. Fig. 4 shows an example of such a case for the triplet 324.1-326.1-326.9 keV. Each of the spectra corresponds to a gate width of two channels in the projection spectrum. This method can be very useful to clarify how complex a line actually is, if this cannot be unambiguously determined from the analysis of singles spectra.

2.4. TIME DISTRIBUTION MEASUREMENTS

In the first set of experiments some runs were devoted to the search of half-lives in the μsec region. No transitions with half-lives greater than a few μsec were found.

TABLE 2

The γ-intensities in coincidence for the set of lines related to the 390.6 keV transition [^{197}Au(α, 3n) $E_\alpha \approx 35$ MeV].

Gate energy (keV) \ E_γ (keV)	122.2	246.0	259.0	296.7	381.1	390.6	401.5	488.6	505.3	647.7	698.0	765.0	791.6
122.2		19	30			86	10						
246.0	71		229	6		225	96				10		
259.0	116	269		48		477	79			57	61	51	
296.7	10	22	26			15	30	w					
381.1						21							
390.6 [b]	200	171	331	26	49		100		54		60		71
401.5	w [c]	59	65	32		61							
488.6		9	9			19							
505.3	10					48	34						
647.7			10			10							
698.0	w	42	38			51		w					
719.0						23							
765.0			18			23							
791.6						19							

[a]) The intensities in coincidence with the 246.0, 259.0 and 390.6 keV γ-rays have errors between 10 and 20 %, the other errors range up to 50 % for the weakest lines.

[b]) This gate has an out-of-beam time window (see fig. 3).

[c]) The symbol w indicates that a weak line is probably present.

TABLE 3

The γ-intensities in coincidence for the set of lines related to the 130.5 keV transition [^{197}Au(α, 3n); E_α = 35 MeV] [a])

E_γ (keV) / Gate energy (keV)	130.5	188.6	196.4	223.0	275.6	279.0	290.5	291.9	303.4	312.6	324.1	326.1	326.9	456.8	472.1	602.4 [g])	603.0	639.5	650.7	778.1
130.5 [b])		w						232				346								
130.5 [c])			180		131	115	134			74	75		157		62	344		w	134	
188.6												180		400						
196.4				300	760	491	898		w	332	503		427			726		280		
223.0			270		123		98			92	144		123		w					
275.6			960	225		232	301		w	169	297		812			204		301	424	
279.0			146		130						279		331		w	204			378	
290.5			508	106	548					731			360		308	521		187		
291.9	150		330	120	337						470		241		79	301			273	
312.6			132		w		258						343			220				
324.1			379	104	308	393		339					292		204	382				
326.1 [d])	481	322	230		225	112	186				165				250					400
326.9 [e])			425	140	371	163	182		w	125	323				254	263				
456.8		284																		250
472.1				232			232			193	258		527					176	355	
602.4 [f])		629		115	94	235	200			125	230		186			484				
603.0 [f])		270			83	69				62			84			215				
639.5		w		171	192		275													
650.7			166		160	158		100												
778.1												267		244						

[a]) Errors range from about 20 % for the strongest lines up to 50 % for the weakest.
[b]) Prompt time window.
[c]) Delayed time window.
[d]) Corresponds to gate 3 of fig. 4.
[e]) Corresponds to gate 4 of fig. 4.
[f]) The two gates correspond to the left and right part of the composite peak.
[g]) It is not possible to resolve the two lines in the coincidence spectra.

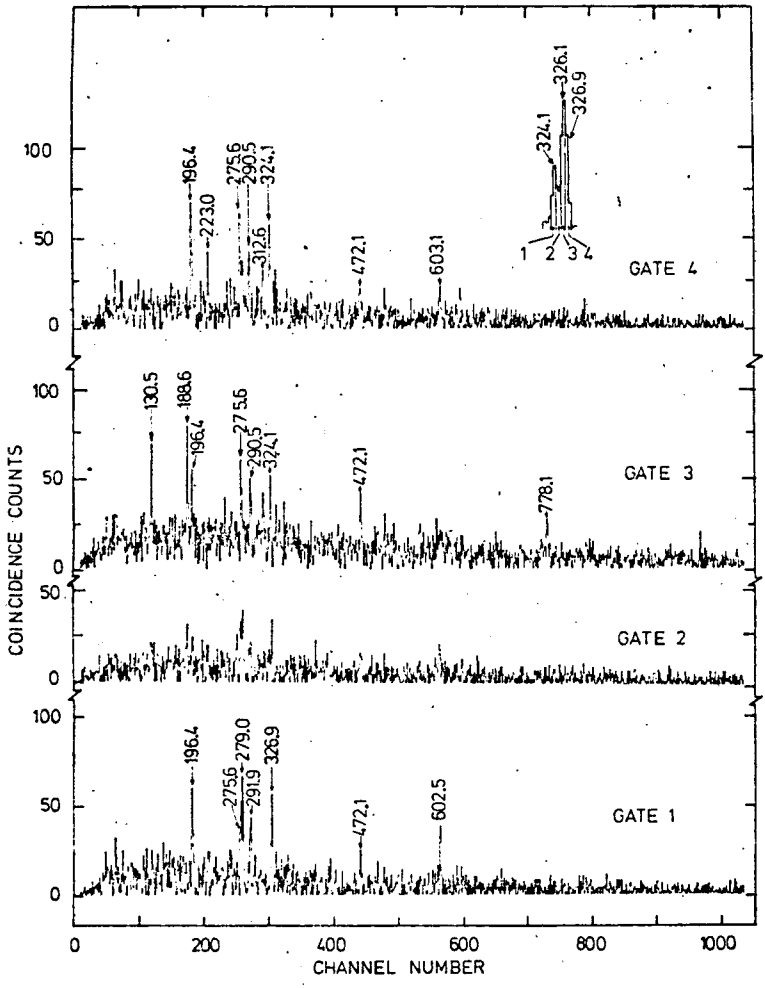

Fig. 4. The γ-γ coincidence spectra corresponding to the gating γ-ray energies given in the insert (see text).

For the nsec region the relevant data are already contained in the measurement discussed in the preceding subsection.

The time distributions of the different γ-rays with respect to each other can be obtained displaying the $t_{\gamma\gamma}$ signals with a gate on a given γ-line in one detector and accepting the entire γ-spectrum in the other. This method is ideal for a case like the 390.6 keV line which directly depopulates an isomeric state and feeds subsequently a very long-lived state (7^+, $T_{\frac{1}{2}} = 1.87$ h). In this case the whole intensity is retarded with respect to all members of the higher lying cascade and no problems of subtraction of prompt components arise. Fig. 5 shows the results for this transition and for comparison a prompt time distribution.

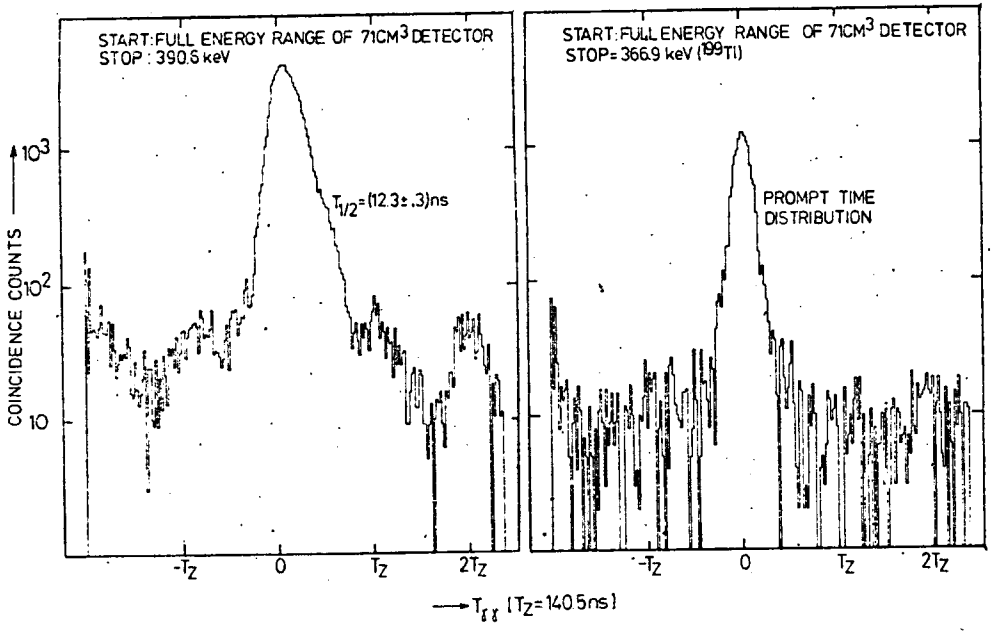

Fig. 5. Two spectra displaying $t_{\gamma\gamma}$ gated on the 390.6 and 366.9 keV transitions. We see at the left side the time distribution of the 12.3 nsec isomeric transition with respect to the intraband γ-rays of the negative parity band; at the right side, for comparison, a prompt time distribution is shown.

It is well known that the measured time distributions represent the convolution between the prompt response of the circuitry and the exponential decay of the delayed radiation. For half-lives comparable to the time resolution of the system the "centroid shift" method [12]) is statistically the best determination of $T_{\frac{1}{2}}$ which leads to 12.3 ± 0.3 nsec.

As also already presented in the preceding subsection there is a γ-ray of 130.5 keV which has transitions both in prompt and delayed coincidence with it. In order to determine the decay constant of the delayed component we set gates on lines which are known to be only in delayed coincidence and follow the intensity of the 130.5 keV radiation as a function of $t_{\gamma\gamma}$. Fitting these numbers with an exponential function we obtain the value $T_{\frac{1}{2}} = 150 \pm 40$ nsec.

2.5. CONVERSION ELECTRON MEASUREMENTS

In-beam γ-ray and conversion-electron spectra were taken at 35 MeV α-particle bombarding energy. The electrons were measured using an iron-free orange-type spectrometer with a momentum resolution around 0.4 %. Further details on the equipment and set-up are given in the literature [13]). Two different runs were made irradiating thin gold foils of 0.6 and 0.3 mg/cm^2, respectively with a beam current of 150 nA. Fig. 6 shows a spectrum which corresponds to the first target. It ranges from $B\rho \approx 1380$ to 2280 G · cm and includes K-shell conversion lines belonging to γ-ener-

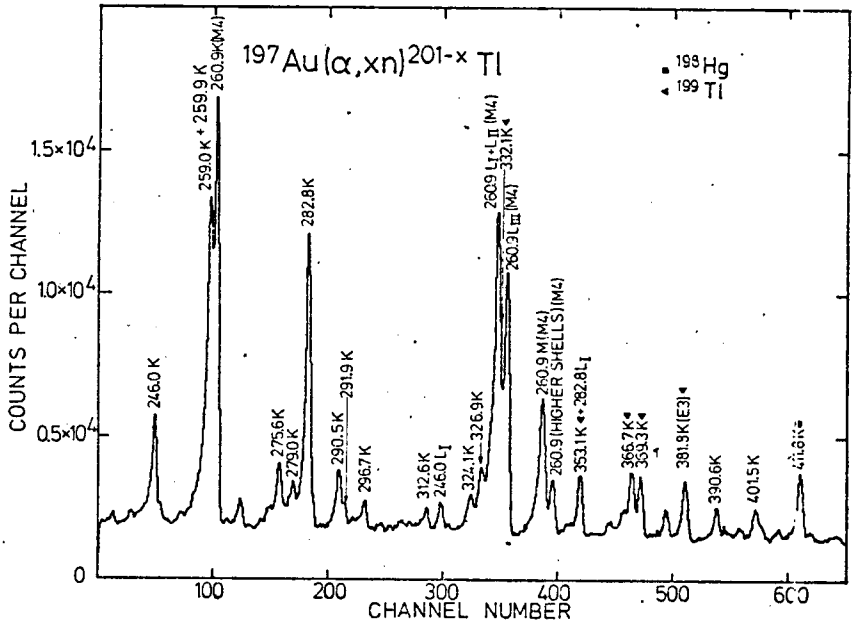

Fig. 6. Conversion-electron spectrum produced by 35 MeV helium ions on a 0.6 mg/cm² ^{197}Au target. Electron lines labelled only with the corresponding γ-energies and an indication of the shell in which they convert belong to ^{198}Tl.

gies between approximately 230 and 420 keV. We obtain the conversion coefficients in this region by normalizing to the known value [5]) for the 381.8 keV E3 transition from the decay of ^{199m}Tl.

The second target was used to cover that energy portion including the L-shell conversion groups of the 122.2 and 130.5 keV transitions. The multipolarity of the 122.2 keV γ-ray was determined from the LI/LII ratio and in turn used as normalization. In this way the results shown in table 4 for the 130.5, 188.6 and 196.4 keV lines were obtained. The accepted character for the transitions follows from both angular distributions and conversion-coefficient data.

5. The level scheme

Part of our preceding knowledge about ^{198}Tl comes from some early work on the electron capture decay of ^{198}Pb [ref. [3])]. Only states with low spins (0^-, 1^-, 2^-) are populated in this process. We fail to observe any of those states. As expected, the (α, xn) reaction leads us to a completely unrelated part of the spectrum. The only data already known at the present time [1, 4]), which also appears in our work, is represented by a long-lived (1.87 h) 7^+ isomer at 543.7 keV and its γ-decay to the ground state. This decay and also the EC branch to ^{198}Hg have been reinvestigated by Pakkanen [14]), so that we consider this part of the scheme as firmly established.

TABLE 4

Conversion electron measurements

E_γ (keV)	α_K [a])	$\alpha_{K,\,theor}$	α_{L_I}	$\alpha_{L_I,\,theor}$	L_I/L_{II}	$(L_I/L_{II})_{theor}$	$\alpha_{K,\,prev.}$ [c])	Accepted multipolarity [d])
122.2				0.639(M1)	7.2	9.78(M1)		M1/E2
130.5			0.55	0.528(M1)	7.6	9.79(M1)		M1-E2
188.6	0.80	1.21(M1)						M1-E2
196.4	1.0	1.08(M1)						M1-E2
246.0	0.52	0.575(M1)						M1/E2
259.0	0.58	0.500(M1)						M1/E2
275.6	0.44	0.421(M1)						M1-E2
		0.079(E2)						
279.0	0.16	0.407(M1)						M1-E2
		0.0768(E2)						
290.5	0.45	0.366(M1)						M1-E2
		0.070(E2)						
291.9	0.36	0.364(M1)						M1-E2
		0.0695(E2)						
296.7	0.52	0.346(M1)						M1/E2
312.6	0.31	0.300(M1)						M1-E2
		0.0589(E2)						
324.1	0.18	0.271(M1)						M1-E2
		0.0539(E2)						
326.1	0.16 [b])	0.265(M1)						M1-E2
326.9		0.0531(E2)						
366.7	0.082	0.19(M1)					0.075±0.02	E2-M1
		0.04(E2)						
369.7	0.14	0.19(M1)					0.17 ±0.03	M1/E2
		0.04(E2)						
381.8		0.098(E3)					0.10 ±0.01	E3
390.6	0.012	0.013(E1)						E1
401.5	0.21	0.15(M1)						M1/E2

[a]) The errors for the conversion coefficients range from 20 to 40 % depending on the intensity and complexity of the line.

[b]) We were not able to resolve this complex line, we quote a "joint" coefficient.

[c]) $\alpha_{K,\,prev.}$ refers to previously measured values [5]), shown for comparison.

[d]) M1/E2 means well known, in general small quadrupole admixtures, whereas M1-E2 indicates somewhat larger δ^2 but not so well determined.

Because of the above mentioned facts we do not expect to reach directly any level lying in between the 7^+ isomer and the ground state. Moreover, this is also supported by the coincidence measurements (gating the 259.9 and 282.8 keV transitions there is nothing in coincidence besides the 260.9 keV γ-ray which depopulates the 7^+ isomer). The 7^+ state represents for us, practically, an effective ground state, with the

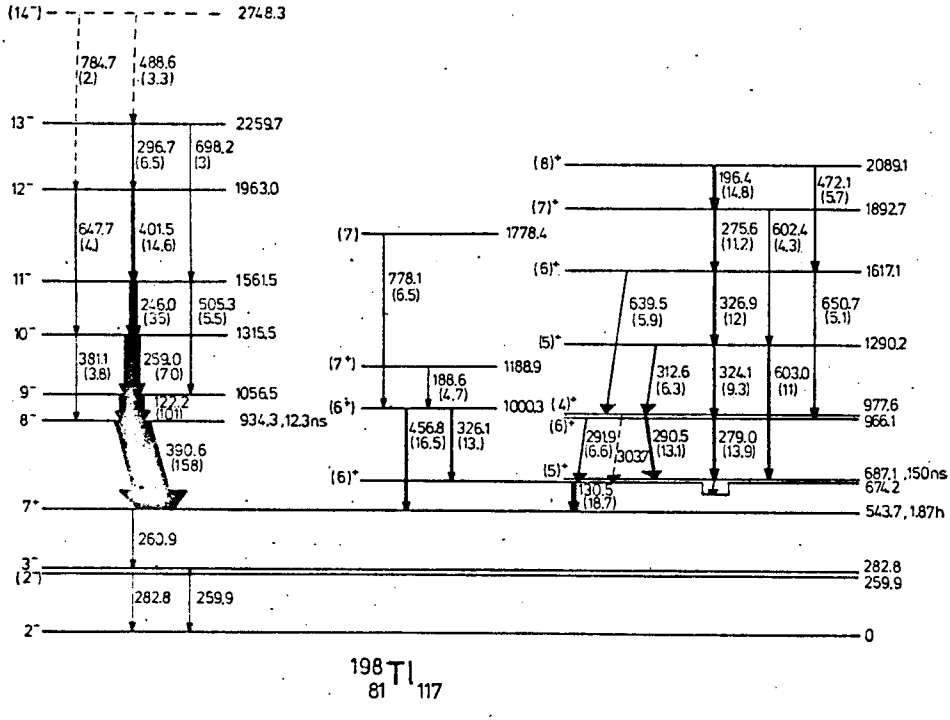

Fig. 7. Level scheme proposed in the present work. The arrow widths for transitions in the negative parity band are proportional to the total transition intensities; for the positive parity part they just reflect the γ-intensities (in this case the mixing ratios are not so well known, see text). The same is valid for the indicated relative intensities.

only difference that we can check the consistency of building up structures on it by means of an intensity balance. We shall come back to this point later.

We show in fig. 7 the level scheme constructed on the basis of the data presented in the preceding section.

Two completely disconnected families of γ-rays were found, we shall therefore divide the following discussion in two parts.

3.1. THE NEGATIVE PARITY BAND

This band is pictured at the left side of fig. 7, the data supporting this scheme are given in tables 2 and 5 and also in fig. 3.

The 390.6 keV γ-ray is by far the strongest line in the spectrum, the rest of the cascade is in delayed coincidence with it and these transitions appear with relative intensities as in the singles spectrum (see fig. 3, first spectrum from below).

These facts firmly establish an isomeric state at 934.3 keV, the half-life of which is measured to be 12.3 $\pm$0.3 nsec.

From a quantitative analysis of the coincidences (table 2) the sequence shown in fig. 7 can be constructed. The angular distributions tell us that all the cascade transi-

tions are of $L = 1$ character with small quadrupole admixtures. The additional assumption of being M1 is necessary to achieve consistency for the proposed partial level scheme. This is specially important in the case of the 122.2 keV transition which should have, if magnetic, a total conversion coefficient of ≈ 5. We shall illustrate this point in the case of the spectrum obtained gating with the 246.0 keV γ-ray. In absence of internal conversion the intensities of the 259.0, 122.2 and 390.6 keV transitions have to be equal. The γ-coincidence intensity of the 259.0 keV line is 229; correcting for internal conversion (and taking into account the measured mixing ratio) we obtain 365 for the total transition strength, which in turn gives 85 (67) for the γ-intensity of the 122.2 keV line (depending on the used mixing ratio, see table 5), as compared to 71 units (measured). The value of 225 for the γ-intensity of the 390.6 keV transition is somewhat low, but the explanation is found in the fact that, because of its lifetime, part of the intensity lies outside the accepted TAC window for prompt coincidences. All cross-over transitions within the band have been found both in singles and coincidence spectra, lending further support to the level ordering.

Concerning the spins of the levels the following can be said. A χ^2 analysis of the angular distributions of the dipole type cascade transitions allows only the possibilities $I \rightarrow I \pm 1$. The minimum χ^2 values for the $I \rightarrow I-1$ option are systematically somewhat smaller than for the $I \rightarrow I+1$ case. Although this difference is not necessary statistically significant, some weak indication can be obtained. There are two additional arguments that favour the monotonic increase of the spin sequence. The first one comes from the excitation function measurements. If the ratio of the γ-yield of the cascade members to the yield of the 390.6 keV transition is plotted against the bombarding energy a constant increase of the slope with increasing α-particle energy in the following order is obtained: 122.2, 259.0, 246.0, 401.5 and 296.7 keV. Also the ratio of I_γ (390.6 keV) to the 7^+ isomer yield increases with energy suggesting a higher spin for the band head.

We can see in table 5 the mixing ratios obtained corresponding to the $I \rightarrow I-1$ assumption. The 390.6 keV γ-ray is a fairly pure dipole, while the intraband transitions have some small, constant, quadrupole admixtures. The increasing anisotropy of the angular distributions (see table 1) as one proceeds towards higher excitation energies, indicates a higher alignment of the states and in turn a higher proximity to the high-spin starting points of the deexcitation process of the compound system (after the emission of the last neutron).

The negative parity of the band results from the conversion-electron measurements (see table 4).

3.2. THE POSITIVE PARITY PART OF THE SPECTRUM

This part of the excitation spectrum is not so strongly populated in our reaction and it is also considerably more complex than the already discussed one. The scheme was constructed in such a way that consistency with the extensive coincidence relations given in table 3 is achieved. It is drawn at the center and right side of fig. 7.

TABLE 5
Level properties for the negative parity cascade

E_{level} (keV)	Energy of depopulating γ-rays (keV)	I_{tot} [a])	δ (δ_{min}; δ_{max})	I^{π}
934.3	390.6	158 ±8	−0.035	8⁻
			(−0.043; −0.023)	
1056.5	122.2 [b])	101 ±5	−0.53	9⁻
			−1.54	
			(−1.65; −0.44)	
1315.5	259.0	70 ±3	−0.16	10⁻
			(−0.17; −0.14)	
	381.1 [c])	3.8±0.6		
1561.5	246.0	35 ±2	−0.16	11⁻
			(−0.18; 0.14)	
	505.3	5.5±0.3		
1963.0	401.5	14.6±0.7	−0.19	
			(−0.21; 0.17)	12⁻
	647.7	4.0±0.4		
2259.7	296.7	6.5±0.4	−0.21	
			(−0.28; −0.14)	13⁻
	698.2	3.0±0.3		
(2748.3)	488.6	3.3±0.3		
				(14⁻)
	784.7	2.0±0.4		

[a]) The errors for the total transition intensity do not include uncertainties in the mixing ratios.
[b]) There are two minima in the $\chi^2(\delta)$ plot below the 0.1 % limit.
[c]) Because of the weakeness of the cross-over transitions, no indication could be obtained from the χ^2 analysis concerning their character or mixing ratios; nevertheless they display positive anisotropy.

The fact that there are some γ-lines in prompt and some other in delayed coincidence with the 130.5 keV γ-ray led us to postulate the unobserved 12.9 keV transition. The 130.5 keV line was scanned channel by channel in order to try to find out if the peak is actually double, but we found the same distribution for the prompt and delayed coincident radiation. Also we did not find a consistent scheme assigning this transition twice. Further weak support is given by the small 303.7 keV cross-over transition.

We have already mentioned that the assumption that all the transitions feed the 7^+ isomeric state has to be checked by means of an intensity balance. The total feeding of the 7^+ state can be obtained in the following way: One has to measure the intensity of the 282.8 keV γ-ray when the irradiated target is in saturation (otherwise corrections have to be made), using then the γ and EC branchings given in ref. [23]), one is able to get this population. We take it to be (100±13) %. The relative partial cross section for the formation of the 8^- state is given by the total transition intensity of the 390.6

TABLE 6

Data from the $\chi^2(\delta)$ analysis for the lines of the positive parity part of the spectrum [a])

E_γ (keV)	I_{total}	Type of transition	δ (δ_{min}; δ_{max})	χ_{min}^2
130.5 [b])	96 ±5	$I \to I \pm 1$	≈0	16.4
188.6	11.5±0.5	$I \to I-1$	−0.14 (−0.21; −0.07)	3.3
		$I \to I+1$	0.21 (0.10; 0.29)	3.3
196.4	23 ±2	$I \to I-1$	−2.47 (−2.74; −2.25)	4.6
		$I \to I+1$	3.49 (3.08; 4.01)	4.6
275.6	16.7±0.7	$I \to I-1$	−0.21 (−0.25; −0.18)	3.5
		$I \to I+1$	0.29 (0.25; 0.32)	3.5
290.5	15.9±0.7	$I \to I-1$	−1.60 (−1.73; −1.38)	5.4
		$I \to I+1$	2.47 (2.24; 2.75)	5.9
291.9	8.3±0.4	$I \to I$	1.11 (0.96; 1.28)	6.9
312.6	7.7±0.4	$I \to I-1$	−1.03 (−1.48; −0.53)	5.0
		$I \to I+1$	1.60 (0.53; 2.05)	5.0
324.1	11.1±0.6	$I \to I-1$	−1.11 (−1.38; −0.58)	5.8
		$I \to I+1$	1.48 (0.62; 1.73)	5.8
326.1 [c])	14.8±1.0	$I \to I$	1.88 (1.60; 2.25)	30
326.9 [c])	13 ±1	$I \to I-1$	−4.01 (−4.70; −3.49)	35
		$I \to I+1$	9.51 (5.67; 14.3)	37
456.9	16.5±1.0	$I \to I-1$	−0.62 (−1.37; −0.49)	2.9
		$I \to I+1$	1.11 (0.67; 1.60)	2.9
472.1	5.7±0.3	A [d])		
602.4	4 ±1	A		
603.0	11 ±1	A		
639.5	5.9±0.5	A		
650.1	5.1±0.5	A		
778.1	6.5±0.5	$I \to I-1$	2.75 (2.05; 4.01)	7.4
		$I \to I+1$	−2.25 (−2.75; −1.73)	7.5

[a]) Only those possibilities are listed for which the χ_{min}^2 value lies below the 0.1 % confidence limit (except in two cases). [b]) See text. [c]) Very degenerate doublet.
[d]) A: In these cases all $\Delta I = 0, \pm 1, \pm 2$ are allowed.

keV γ-ray and represents $(50\pm4)\,\%$; we obtain also $(32\pm3)\,\%$ for the 130.5 keV and $(6\pm0.5)\,\%$ for the 456.8 keV transition. We see that there is no contradiction on this point.

The relevant data for the discussion of the spin assignments are collected in table 6. Only those possibilities are listed for which the χ^2 lies below the 0.1 % confidence limit (except for two cases), the other ones have in general χ^2 values one to three orders of magnitude larger. Due to the greater complexity of this part no unique values for the spins can be obtained. Let us now discuss briefly the different possibilities.

Levels at 674.2 and 1000.3 keV. The first level decays to the 7^+ isomer by means of the 130.5 keV γ-ray. This line shows the smallest anisotropy among the measured stretched dipole-type transitions (see table 1). This is obviously due to the fact that a considerable amount of its intensity goes through the 150 nsec isomeric state. We assume that for practical purposes this part is completely attenuated. In order to investigate the character of the transition this isotropic contribution has been subtracted, transforming into γ-intensity the total intensity of the 603.0, 279.0 and 290.5 keV transitions. This has to be done in an iterative way because the unknown mixing ratio enters in this calculation. The smallest χ^2 has been found for a fairly pure magnetic dipole ($\delta \approx 0$). This fact would give us the options 6^+ or 8^+ for the I^π of the level in question. Another argument supports this assignment: The 456.8 keV transition is of $I \rightarrow I\pm1$ type, which gives spin 6 or 8 for the level at 1000.3 keV. This level decays also by means of the 326.1 keV line to the level in discussion. This line is very degenerate with another of 326.9 keV and it is admittedly hard to separate them, although this can be done and the $I \rightarrow I$ option is strongly favoured over all the others. In addition the M1/E2 character for the 130.5 keV comes out from the conversion-electron measurements.

The 291.9 keV line, which is in prompt coincidence with the 130.5 keV γ-ray, has $I \rightarrow I$ character; regarding the possible spin values for the level at 647.2 keV we also obtain 6 or 8 for the present one. The four lines of 290.5, 279.0, 312.6. and 324.1 keV are of the $\Delta I = 1$ type. Unfortunately there are not enough statistics to obtain a definitive answer about the character of the cross-overs, in particular the two transitions of 603.0 and 602.4 keV are also very degenerate and a χ^2 analysis leaves the question completely open, except for the limitation $|\Delta I| \leqq 2$. The allowed combinations (listed in the level order within each of them) would be 5, 6, 4, 5; 5, 6, 6, 7(5); 7, 6, 6, 7(5); 7, 6, 8, 7; 7, 8, 6, 7, 7, 8, 8, 9(7); 9, 8, 8, 9(7); 9, 8, 10, 9. From here on only weak arguments can be made. Due to the fact that the branching from the 150 nsec state to the 7^+ isomer is not observed, we shall try to keep the spin difference between them as large as possible. Analogous arguments can be made for the state at 977.6 keV. The cross-over transition to the 674.2 keV state (parallel to the 291.9 keV line) is in the best case very weak. This would probably suggest that the two nearby states do not have the same spin. In addition, the fact that the population of this part of the spectrum is much weaker than for the negative parity band leads to

choose the first one of the above mentioned combinations as the best candidate. It is just in this spirit that the tentative assignments shown in fig. 7 have to be considered.

For the levels at 1617.1, 1892.7 and 2089.1 keV, all the transitions connecting them are of $\Delta I = 1$ type. For similar reasons as given in the preceding subsection we shall propose a normal increasing spin sequence (6, 7, 8).

The positive parity of this part is also firmly supported by the measured conversion coefficients.

4. Interpretation of the measurements

4.1. RELEVANT DEGREES OF FREEDOM

As mentioned in the introduction, Tl isotopes display a very interesting feature, namely the transition from a spherical to a deformed shape, above a certain excitation energy for some specific families of states.

The low-energy low-spin part of the spectra in both odd-even (o-e) and doubly odd (o-o) isotopes can be accounted for in simple spherical shell-model terms [2, 15, 16]).

The relevant single-particle excitations for the discussion of this part are those arising from $s_{\frac{1}{2}}$ and $d_{\frac{3}{2}}$ (positive parity) and $h_{\frac{11}{2}}$ (negative parity) orbitals for the protons and from $p_{\frac{1}{2}}$, $p_{\frac{3}{2}}$, $f_{\frac{7}{2}}$ (negative parity) and $i_{\frac{13}{2}}$ (positive parity) for the neutrons.

The $s_{\frac{1}{2}}$ proton appears as the ground-state configuration in odd-mass thallium nuclei; the first excited states being $\frac{3}{2}^+$ can be identified as a hole in the $d_{\frac{3}{2}}$ orbital. As long as the odd proton remains in the major shell ending at $Z = 82$ we have to deal with a single hole in a lead core. The lowest excitation of this doubly even core is a 2^+ quadrupole phonon at approximately 1 MeV. The properties of the low-lying $\frac{5}{2}^+$ second-excited states in o-e Tl can be reproduced by coupling the $s_{\frac{1}{2}}$ proton to this phonon. This was done by several authors in the framework of the particle-vibration coupling scheme [17, 18]) and in the pairing-plus-quadrupole [19]) model. In this situation the pairing force only can be effective for the neutrons.

The first $\frac{11}{2}^-$ state of non-collective nature (the meaning of this statement will become clear shortly) does not appear below 1.3 MeV and can be identified as the opposite parity $h_{\frac{11}{2}}$ hole. The available data [20]) are given in table 7; as we can see there the excitation energy of this degree of freedom remains constant over a wide range of mass numbers (although the systematics are not complete).

At the neutron side, we have in the odd lead isotopes the systematic appearance of low-lying negative parity states $\frac{5}{2}^-$, $\frac{3}{2}^-$ and $\frac{1}{2}^-$. If we take as a starting point, the spherical single-particle energies as given by McGrory and Kuo [21]), the experimental sequence can be reproduced with the aid of a pairing force. The independent fermionic excitations are then properly described by BCS quasiparticles. For instance, the bare particle $p_{\frac{1}{2}}$ energy lies below that for $f_{\frac{5}{2}}$. After turning on the interaction the occupation number distribution is no longer sharp and the Fermi level is pushed up so that the $\tilde{f}_{\frac{5}{2}}$ quasiparticle becomes the ground state of the lead isotopes in the mass region around 200. Also the compression of the quasiparticle spectrum as compared with the independent particle spacings is found in the data.

TABLE 7

Systematics for $\tilde{\nu}(i_{13/2}\text{-}f_{5/2})$, $7^+\text{-}2_1^-$ and $\tilde{\pi}(h_{9/2}\text{-}s_{1/2})$ energy differences

A (Pb)	A (Tl)	A (Hg)	$E(\frac{13}{2}^+\text{-}\frac{5}{2}^-)$ (Pb) (MeV)	$E(7^+\text{-}2_1^-)$ (Tl) (MeV)	$E(\frac{13}{2}^+\text{-}\frac{1}{2}^-)$ (Hg) (MeV)	$E(\frac{11}{2}^-\text{-}\frac{1}{2}^+)$ (Tl) (MeV)
	207					1.341
207	206		1.064	1.357		
205	204		1.014	1.118		
	203					1.47
203	202		0.825	0.950		
201	200	201	0.629	0.752	$\approx$ 0.750	
	199					(1.394)
199	198	199	0.424	0.543	0.374	
197	196	197	0.234	0.395	0.165	

At somewhat higher energy the $i_{13/2}$ even parity orbital comes into play showing a monotonic decrease with decreasing mass number (see table 7). The situation here is very different to that encountered for protons, because in going to the neutron deficient side one is removing particles from the $p_{1/2}$, $f_{5/2}$ and $p_{3/2}$ levels and the Fermi surface approaches the $i_{13/2}$ state. Taking into account the above mentioned degrees of freedom it is easy to discuss the already known low-energy part of the spectra in o-o thallium nuclei. The low-spin negative parity states can be constructed by coupling the low-spin even-proton states to the low-spin odd parity neutrons. For instance, the ground states are expected to be mainly $[\tilde{\pi}s_{1/2} \otimes \tilde{\nu}f_{5/2}]_{2^-}$, although some configuration mixing is likely to be present [2, 16]). Positive parity of low-lying states in o-o Tl nuclei can result from the coupling between a neutron of odd parity and $\tilde{\pi}h_{9/2}$ or a proton of even parity and $\tilde{\nu}i_{13/2}$. In this way high-spin levels of positive parity may arise. The lowest states of this kind are certainly those of the second type, because of the much higher energy required to excite the $\tilde{h}_{9/2}$ hole. Let us suppose that the dominant component of the 7^+ isomeric states is $[\tilde{\pi}s_{1/2} \otimes \tilde{\nu}i_{13/2}]_{7^+}$. If this would be the case the level spacing $7^+\text{-}2_1^-$ should vary with mass number in approximately the same way as the $\tilde{i}_{13/2}\text{-}\tilde{f}_{5/2}$ spacing in the odd lead isotopes. The experimental situation is also displayed in table 7. As we can see both variation and magnitude of the spacings are very similar for the same number of neutrons, which supports the interpretation given above.

Now, when the odd proton jumps to the next higher-lying major shell the situation changes in a rather drastic way. We are left with a Hg core and the extra polarizing effects of the particle in the high-j shell. Looking at the Nilsson diagram [22]) at the $Z = 82$ shell closure one can see that in going to oblate shapes energy is gained from two sources: first the $h_{9/2}^-$ [505] state comes down and second the level density in the vicinity of the Fermi surface increases allowing the development of pairing correlations (even when it is not clear to what extent) [5]). In addition, microscopically

calculated potential energy surfaces suggest some tendency to oblate shapes [23]). So-called strongly coupled bands based on this $\tilde{h}_{\frac{9}{2}}$ proton were in fact shown to exist [5, 6]) in all neutron deficient odd-mass thallium nuclei below mass 200. Even when this band is strongly distorted by the Coriolis interaction, the situation is such that at the beginning of the band the coupling to the deformed potential dominates the decoupling tendency of this force [7]). The proton has hence a fairly well defined projection of its angular momentum along the symmetry axis, specifically the maximum possible one, so that its j points in this direction. We also try to describe this band in the framework of the particle-vibration coupling model in the QRPA approximation including third-order anharmonicities [24, 25]) but it has recently become clear that higher-order terms are required in order to reproduce the experimental data [26]).

In front of the above situation it is pertinent to review briefly some facts of the odd Hg isotopes.

We encounter here systematically low-lying $\frac{1}{2}^-$, $\frac{5}{2}^-$ and $\frac{3}{2}^-$ states, the ordering of which can be reproduced if one assumes some small oblate deformation. The quasiparticles associated with the $\frac{1}{2}^-[501]$, $\frac{5}{2}^-[503]$ and $\frac{3}{2}^-[501]$ Nilsson states will respectively provide the basis for such an explanation. This holds even when the blocking of the odd particle is taken into account.

The next feature to be mentioned is the appearance of $\frac{13}{2}^+$ states, recognized as the lowest members of decoupled bands on an $\tilde{i}_{\frac{13}{2}}$ quasineutron with its angular momentum completely aligned with the rotation axis [27]). The variation with mass number of the excitation energy of these $\frac{13}{2}^+$ states is again indicated in table 7 and is also found to be similar to the situation in odd lead nuclei.

In view of the facts presented so far and the success of the particle-plus-rotor model in reproducing the rotational structures in odd mass transitional nuclei we will search, also in the doubly odd case, within this framework for a description of our experimental results.

4.2. THE MODEL

The system's Hamiltonian is that of the particle-plus-rotor model for the case of two out-of-core particles [see for instance, ref. [22]), p. 85]. The configuration space for the intrinsic motion is spanned by allowing both protons and neutrons to move in two sets of specific Nilsson orbits. In addition, a pairing interaction for each type of particle is separately taken into account and treated in the BCS approximation. The two well known superconducting equations were solved for each value of the deformation β. For this purpose, all Nilsson states belonging to the major shells below and above $Z = 82$ and $N = 126$ respectively were taken into account. The pairing strength for neutrons, for which these effects are significant, was taken so as to give a gap of ≈ 0.7 MeV, of the order of the odd-even mass differences in this region; for protons we take $G_p \approx 0.13$ MeV (this point will be discussed in some detail later). This procedure gives us the Fermi level, the quasiparticle energies and

the occupation amplitudes which are in turn used to calculate the reduction factors for the Coriolis matrix elements.

The resulting intrinsic states are then product states of a quasineutron and a quasiproton which retain the quantum numbers of the Nilsson particles. No residual interaction is considered between the valence particles. We only treat the rotational degree of freedom of the core. The basis states for the whole system are then

$$|IMK_>(\Omega_n, \Omega_p)\rangle = N\{D^I_{MK_>}\alpha^\dagger_n(\Omega_n)|\mathrm{BCS}\rangle_n\alpha^\dagger_p(\Omega_p)|\mathrm{BCS}\rangle_p + (-1)^{I+K}D^I_{M-K_>}\alpha^\dagger_n(\bar{\Omega}_n)|\mathrm{BCS}\rangle_n\alpha^\dagger_p(\bar{\Omega}_p)|\mathrm{BCS}\rangle_p\} \quad (K_> = \Omega_n+\Omega_p),$$

$$|IMK_<(\Omega_n, \Omega_p)\rangle = N\{D^I_{MK_<}\alpha^\dagger_n(\Omega_n)|\mathrm{BCS}\rangle_n\alpha^\dagger_p(\bar{\Omega}_p)|\mathrm{BCS}\rangle_p + (-1)^{I+K+1}D^I_{M-K_<}\alpha^\dagger_n(\bar{\Omega}_n)|\mathrm{BCS}\rangle_n\alpha^\dagger_p(\Omega_p)|\mathrm{BCS}\rangle_p\}$$

[e.g. $\Omega_p \leqq \Omega_n$; $K_< = |\Omega_n-\Omega_p|$; $N = ((2I+1)/16\pi^2)^{\frac{1}{2}}$] with energies $E_n(\Omega_n)+E_p(\Omega_p)+(\hbar^2/2\theta)\,(I(I+1)-K^2)$. The quantities Ω_n and Ω_p are always taken to be positive and the Bohr and Mottelson [28]) sign conventions are used throughout. Operators $\alpha^\dagger_n(\Omega_n)$ [$\alpha^\dagger_p(\Omega_p)$] create a quasineutron [proton] in a state characterized by the quantum numbers n, Ω_n (p, Ω_p). Further, $E_n(\Omega_n)$ and $E_p(\Omega_p)$ are the quasiparticle energies and $\hbar^2/2\theta$ has been calculated using the traditional Grodzins relation, $\hbar^2/2\theta = 204\,\beta^{-2}\,A^{-\frac{7}{3}}$ [ref. [8])].

In this basis we diagonalize the particle-rotation coupling term which in our case takes the form

$$H_{\mathrm{prc}} = -(\hbar^2/2\theta)\{(I^+J^- + I^-J^+) + (j^+_p j^-_n + j^-_p j^+_n) + (j^+_p j^-_p - j_{3p} + j^+_n j^-_n - j_{3n})\} \quad (J = j_p + j_n).$$

Only the one-quasiparticle part of the operators are effectively used because we always restrict ourselves to systems of two independent quasiparticles. The last coupling term is written in a somewhat unusual manner to indicate that it has nondiagonal matrix elements between different Nilsson states provided they have the same Ω. Due to the fact that the stepping operators are only able to connect Nilsson orbits of the same parity, our configuration space divides naturally into several systems. In first place the systems $\tilde{\pi}\mathrm{h}_{\frac{9}{2}} \otimes \tilde{\nu}\mathrm{i}_{\frac{13}{2}}$ and $\tilde{\pi}\mathrm{h}_{\frac{9}{2}} \otimes \tilde{\nu}(\mathrm{p}_{\frac{1}{2}}, \mathrm{f}_{\frac{7}{2}}, \mathrm{p}_{\frac{3}{2}})$ were investigated. In both cases the odd proton lies in the single-j shell $\mathrm{h}_{\frac{9}{2}}$: in the first one the neutron is also in a single-j shell and in the second one the neutron is allowed to move in the six low-spin odd parity Nilsson orbitals arising from the spherical $\mathrm{p}_{\frac{1}{2}}$, $\mathrm{f}_{\frac{7}{2}}$ and $\mathrm{p}_{\frac{3}{2}}$ shell-model states.

These two systems, according to our previous discussion, are expected to play the important role in o-o thallium. Also, the systems $\tilde{\pi}\mathrm{h}_{\frac{11}{2}} \otimes \tilde{\nu}\mathrm{i}_{\frac{13}{2}}$ and $\tilde{\pi}(\mathrm{s}_{\frac{1}{2}}, \mathrm{d}_{\frac{3}{2}}) \otimes \tilde{\nu}\mathrm{i}_{\frac{13}{2}}$ were calculated to see how the resulting structures will look like if Tl nuclei would actually assume an oblate deformation in such a situation. The second system here has also to be understood as the coupling of the proton moving in the three Nilsson states originating in the $\mathrm{s}_{\frac{1}{2}}$ and $\mathrm{d}_{\frac{3}{2}}$ shell-model states and $\tilde{\nu}\mathrm{i}_{\frac{13}{2}}$. The whole calculation

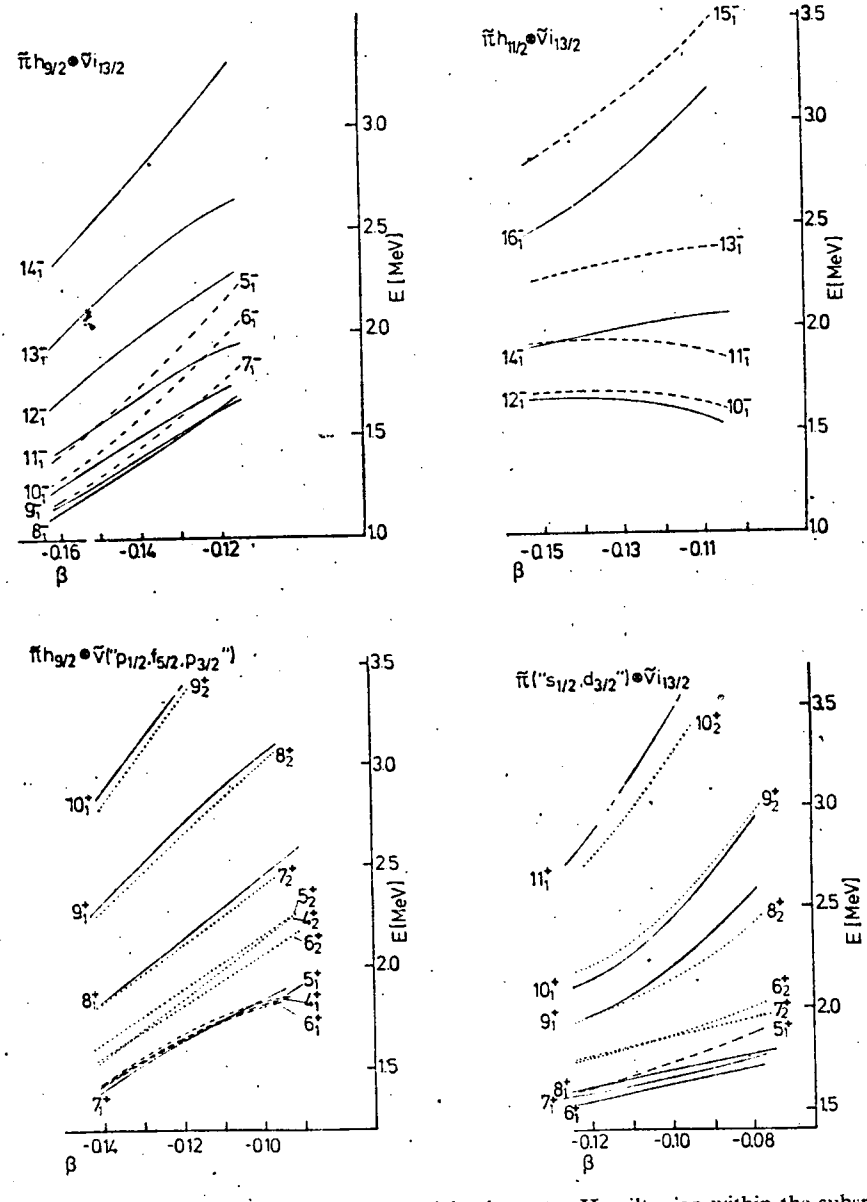

Fig. 8. Level sets obtained diagonalizing the particle-plus-rotor Hamiltonian within the subspaces spanned by $\tilde{\pi}h_{\frac{1}{2}}\otimes\tilde{\nu}i_{\frac{1}{2}}$; $\tilde{\pi}h_{\frac{1}{2}}\otimes\tilde{\nu}i_{\frac{13}{2}}$; $\tilde{\pi}h_{\frac{9}{2}}\otimes\tilde{\nu}(p_{\frac{1}{2}}, f_{\frac{5}{2}}, p_{\frac{3}{2}})$; $\tilde{\pi}(s_{\frac{1}{2}}, d_{\frac{3}{2}})\otimes\tilde{\nu}i_{\frac{13}{2}}$ (wavy lines over π and ν denote as usual quasiparticle states).

has essentially only one free parameter, namely the quadrupole deformation β. No effort was invested in the optimization towards quantitative agreement with the data because we are interested in qualitative features and also do not expect such an agreement to be other than fortuitous in the framework of our simple model. Blocking

effects were investigated and it was found that even though the pairing correlations are somewhat reduced no substantial modification of the results takes place.

The results for these four systems are presented in fig. 8, where mainly the excitations energies of the yrast states are displayed as functions of β. The energies are intercomparable for each deformation, they represent excitation energies on the ground state of the ^{196}Hg core. Let us discuss now in somewhat more detail the different systems.

4.2.1. The $\tilde{\pi}h_{\frac{9}{2}} \otimes \tilde{\nu}f_{\frac{7}{2}}$ and $\tilde{\pi}(s_{\frac{1}{2}}, d_{\frac{3}{2}}) \otimes \tilde{\nu}i_{\frac{13}{2}}$ systems. The first system represents the best candidate to give the yrast sequence in o-o thallium, and therefore should receive the strongest feeding in (α, xn) experiments.

This system was treated in the single-j-shell approximation. The proton was allowed to move in the five Nilsson states arising from the magnetic substates of $h_{\frac{9}{2}}$ and the neutron in the seven states arising from $i_{\frac{13}{2}}$, this produces then seventy different intrinsic states by parallel and antiparallel addition of the corresponding angular momentum projections ($K_z = |\Omega_n \pm \Omega_p|$). The results of the diagonalization of H_{prc} within this subspace are shown in the upper left of fig. 8, we see, for $I \geqq 5$, the state of lowest energy (smaller spins lie even higher). Yrast states are characterized by solid lines; a band with a normal spin sequence ($\Delta I = 1$) develops based on the 8_1^- level practically over the whole range of deformation. This range was selected around the best values found for the odd mass Tl isotopes [8]). The second excited states for each spin are not shown because they appear above the 12_1 state and are therefore not expected to have experimental relevance in our case. The wave functions for the yrast states display the following features. At the beginning of the band the proton remains in a relative pure $\Omega_p = \frac{9}{2}$ state. With increasing spin, where the Coriolis effects are stronger, the admixture of lower Ω_p components becomes more and more important, reflecting the decoupling tendency. For the neutron, as expected, the situation is very different. Throughout the whole band several Ω_n components are considerably admixed, with a fairly constant distribution centered around $\Omega_n = \pm\frac{1}{2}$ reflecting here the fact that the quasineutron j is aligned with the rotation axis. In this form the coupling at a right angle of proton and neutron angular momenta becomes the energetically most favourable one, making the 8_1^- state the band head of this system. We show in fig. 9 a comparison between the calculation and the measured negative parity band. The energies labelling these levels represent the spacings between adjacent states (i.e. the transition energies for $I \to I-1$), for the calculation we have chosen the numbers at $\beta = -0.15$. As can be seen some qualitative features are well reproduced. The ordering is the right one and the small distance between the first two members as compared with the other spacings in the band comes out. The relatively small spacings of the first steps as compared with the measured ones are probably due to a residual p-n interaction, neglected in the calculation, which splits the different J-values ($J = j_p + j_n$). This could happen if the structure of the intrinsic state changes to some extent as one proceeds in the band. Even though some staggering of the levels is present in the calculation, it is a very much pronounced effect in the experimental sequence and

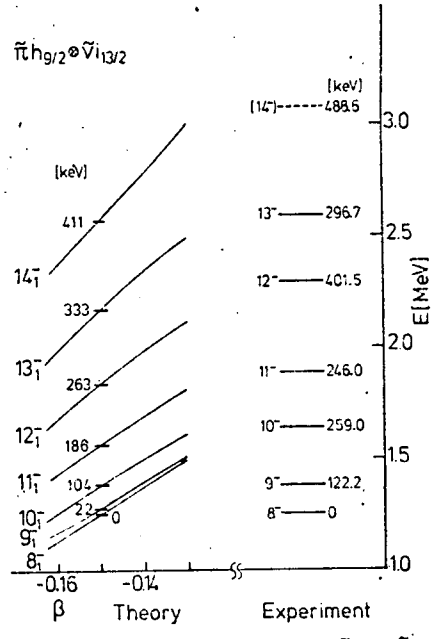

Fig. 9. Comparison between the calculated yrast states for the $\tilde{\pi}h_{\frac{1}{2}}\otimes\tilde{\nu}i_{\frac{1}{4}}$ system and the measured negative parity band. We indicate the transition energies corresponding to $\beta = -0.15$ against the measured ones.

we expect such a feature to be correctly described if the core is allowed to assume asymmetric shapes. This is the case in the odd thallium nuclei where Meyer-ter-Vehn [8]) found a value near 40° for the γ-deformation.

In addition we have tried to understand the large hindrance factor of the E1 transition depopulating the 8^- isomeric state in the framework of this model. For this reason let us briefly discuss the $\tilde{\pi}(s_{\frac{1}{2}}, d_{\frac{1}{2}}) \otimes \tilde{\nu}i_{\frac{1}{4}}$ system which is shown in the lower right of fig. 8. Although it is not justified to undertake a detailed comparison between the calculation and the experiment, because of the incompleteness of the latter information, we can see that the level density is much higher at the beginning of this structure as compared to the one already discussed. The 7_1^+ state lies very near to the bottom of this system and even though we have not shown the I_3 states there is a 6_3^+ and a 7_3^+ state lying in between the 6_2^+ and 8_2^+ states; in principle there are enough states to account for the set of transitions promptly related to the 130.5 keV line depicted at the center of fig. 7.

If the 7_1^+ state (from now on identified with the 7^+ isomeric state) were completely spherical, the transition from the 8^- state would be absolutely forbidden. On the other hand, if the assumption is made that this state actually adopts a small deformation the transition becomes possible. The measured hindrance factor relative to the single-particle value is $\approx 2 \times 10^{-7}$; we were able to get a similar retardation ($\approx 3 \times 10^{-6}$) assuming a value of $\beta = -0.08$. It must be said, however, that this

result depends sensitively on the detailed structure of the levels in the vicinity of the proton Fermi level and on the magnitude of the pairing strength which in turn determine the effectiveness of this force. Taking the level sequence given in ref. [22]) the superconducting solution begins to develop at $G_p = 0.132$ MeV $(26.2/A$ MeV), the transition between the normal and superfluid systems is very sharp and takes place in a very small range of G_p, resulting in a variation of the hindrance factor from 10^{-5} to zero. Playing around with the value of β and /or G_p the experimental value can certainly be reproduced, but more interesting than that is to look at the different causes contributing to the hindrance. They can be easily understood if one remembers the selection rules for the E1 operator. The values $\Delta\Omega_p = \pm 1, 0$ imply that the transition can only proceed through the small admixtures of low Ω_p components $(\Omega_{p,i} \leqq \frac{5}{2})$ into the wave function of the 8^- state caused by the Coriolis force. The values $\Delta j_p = \pm 1, 0$ mean that only the high-j $(j_{p,f} = \frac{7}{2}, \frac{9}{2})$ amplitudes of the Nilsson states, arising from the $s_{\frac{1}{2}}$ and $d_{\frac{3}{2}}$ orbitals, in the final state will contribute. This coefficients are known to be small and are functions of β. Additional hindrance comes from the pairing factor $u_1u_2 - v_1v_2$ appropriate to reduce the single-particle matrix elements when one-quasiparticle states are connected, it is clear that a very sharp Fermi surface would suppress the transition.

4.2.2. The $\tilde{\pi}h_{\frac{9}{2}} \otimes \tilde{\nu}(p_{\frac{1}{2}}, f_{\frac{5}{2}}, p_{\frac{3}{2}})$ system. This structure is also shown in fig. 8, similar remarks as those concerning the $\tilde{\pi}(s_{\frac{1}{2}}, d_{\frac{3}{2}}) \otimes \tilde{\nu}i_{\frac{13}{2}}$ can also be made in this case. The incomplete experimental information makes the comparison between theory and experiment very speculative. Again here, there are enough states to allow in principle an interpretation in these terms of the structure constructed on the 150 nsec isomer. A 5_1 level is among the lowest states, 4_2 approaches 6_2 around $\beta = -0.14$, and, although not shown, 4_3 and 5_3 are near and below 7_2, and 6_3 and 7_3 (in this order) in between 8_1 and 8_2. Additional complication is expected in this case where a residual p-n interaction could mix this system with $\tilde{\pi}(s_{\frac{1}{2}}, d_{\frac{3}{2}}) \otimes \tilde{\nu}i_{\frac{13}{2}}$ (also of positive parity).

4.2.3. The $\tilde{\pi}h_{\frac{9}{2}} \otimes \tilde{\nu}i_{\frac{13}{2}}$ system. This case is shown in the upper right of fig. 8. Due to the fact that in our case both orbitals lie well below the corresponding Fermi levels, the two quasiparticles are completely aligned with the rotation axis giving the maximum possible angular momentum (12_1^-) and a decoupled band develops on top of this state (the "favoured states" 12_1^-, 14_1^- and 16_1^- are indicated by solid lines). Such a situation is expected to be found in nuclei with more proton holes in the shell ending at $Z = 82$, than in the thallium case.

5. Conclusion

Relative simple and pure structures are shown to survive in ^{198}Tl, in spite of the expected complexity of the excitation spectrum of heavy mass o-o nuclei.

High-j, unique parity orbitals seem to play, also in o-o transitional nuclei, an important role. Strong Coriolis effects are found to be present, as in the odd mass thallium case, and probably dominate the neglected residual p-n interaction. In

addition shape coexistence phenomena are very likely to show up. Further work is in progress towards the better understanding of these various interesting features.

We are greatly indebted to many people for valuable discussions and encouraging support for this project. Among these are D. R. Bès, G. G. Dussel, C. Günther, G. Holzwarth, H. Hübel, P. Kleinheinz, R. M. Lieder, M. R. Maier, H. J. Mang, H. Morinaga, C. Pomar, P. Ring, O. W. B. Schult, F. S. Stephens and H. Toki. One of us (A.J.K.) wants to acknowledge sincerely the hospitality at the E17 Institute of the Technical University Munich and the financial support by the DAAD (Deutscher Akademischer Austauschdienst).

References

1) B. Jung and G. Andersson, Nucl. Phys. **15** (1960) 108
2) R. E. Doubler, Wm. C. McHarris and W. H. Kelly, Phys. Rev. C2 (1970) 2422
3) B. Jung, Nucl. Phys. **10** (1959) 440
4) R. M. Diamond and F. S. Stephens, Nucl. Phys. **45** (1963) 632
5) J. O. Newton, S. D. Cirilov, F. S. Stephens and R. M. Diamond, Nucl. Phys. **A148** (1970) 593
6) J. O. Newton, F. S. Stephens and R. M. Diamond, Nucl. Phys. **A236** (1974) 225
7) F. S. Stephens, Rev. Mod. Phys. **47** (1975) 43 and references therein
8) J. Meyer-ter-Vehn, F. S. Stephens and R. M. Diamond, Phys. Rev. Lett. **32** (1974) 1383
9) H. E. Kurz, E. W. Jasper, K. Fischer and F. Hermes, Nucl. Phys. **A168** (1971) 129
10) H. M. Jäger, H. Beuscher, W. F. Davidson, R. M. Lieder and A. Neskakis, Nucl. Instr. **125** (1975) 53
11) J. Gizon, A. Gizon, M. R. Maier, R. M. Diamond and F. S. Stephens, Nucl. Phys. **A222** (1974) 557
12) R. E. Bell, in Alpha-, beta- and gamma-ray spectroscopy, vol. 2, ed. K. Siegbahn (North-Holland, Amsterdam, 1965) p. 921
13) W. D. Schneider and K. H. Gonsior, Nucl. Instr. **130** (1975) 165
14) A. Pakkanen, Nucl. Phys. **A172** (1971) 193
15) I. Bergström and G. Anderson, Ark. Fys. **12** (1957) 415
16) A. de-Shalit and J. D. Walecka, Nucl. Phys. **22** (1961) 184
17) A. Covello and G. Sartoris, Nucl. Phys. **A93** (1967) 481
18) G. Alaga and G. Ialongo, Nucl. Phys. **A97** (1967) 600
19) L. S. Kisslinger and R. A. Sorensen, Rev. Mod. Phys. **35** (1963) 853
20) Nuclear level schemes $A = 45$ through $A = 257$ from Nucl. Data Sheets, ed. Nucl. Data Group (Academic Press, New York, 1973)
21) J. B. McGrory and T. T. S. Kuo, Nucl. Phys. **A247** (1975) 283
22) J. P. Davidson, Collective models of the nucleus (Academic Press, New York, 1968) p. 186
23) K. Kumar and M. Baranger, Nucl. Phys. **A110** (1968) 529
24) D. R. Bès and G. G. Dussel, Nucl. Phys. **A135** (1969) 1
25) D. R. Bès and G. G. Dussel, Nucl. Phys. **A135** (1969) 25
26) V. Paar, in Proc. Topical Conf. on problems of vibrational nuclei, Zagreb, 1974, ed. G. Alaga, V. Paar and L. Sips (North-Holland, Amsterdam, 1975) p. 15
27) D. Proetel, D. Benson, Jr., A. Gizon, J. Gizon, M. R. Maier, R. M. Diamond and F. S. Stephens, Nucl. Phys. **A226** (1974) 237
28) A. Bohr and B. R. Mottelson, Nuclear structure, vols. 1 and 2 (Benjamin, New York, 1969 and 1975)